

Inverse Seesaw Mechanism and Axion Portal Fermionic Dark Matter

Nakorn Thongyoi,^a Patipan Uttayarat,^b and Chakrit Pongkitivanichkul^a

^a*Khon Kaen Particle Physics and Cosmology Theory Group (KKPaCT),
Department of Physics, Faculty of Science, Khon Kaen University,
123 Mitraphap Rd, Khon Kaen 40002, Thailand*

^b*Theoretical High-Energy Physics and Astrophysics Research Unit (ThEPA), Department of Physics,
Srinakharinwirot University, 114 Sukhumvit 23 Rd.,
Wattana, Bangkok 10110, Thailand*

E-mail: nakorn.thongyoi@gmail.com, patipan@g.swu.ac.th,
chakpo@kku.ac.th

ABSTRACT: We propose a minimal extension of the Standard Model (SM) that addresses both the smallness of neutrino masses and the dark matter (DM) puzzle via the inverse seesaw mechanism and an axion portal fermionic DM. This model generates light neutrino masses without requiring high energy scales, enhancing its testability in future collider experiments. An axion-like particle (ALP) connects the SM and DM sectors, yielding a distinct phenomenology and a positive contribution to the muon anomalous magnetic moment ($g - 2$) anomaly. Our analysis shows that the model is consistent with constraints from neutrino oscillations, DM relic density, and indirect detection, as well as providing a solution to the $g - 2$ anomaly. The TeV-scale scalar sector and ALP interactions suggest potential signals in collider experiments and astrophysical observations. This work offers a unified framework to address neutrino masses and DM, with implications for particle physics and cosmology.

Contents

1	Introduction	1
2	The model	3
2.1	The scalar sector	3
2.2	The neutrino sector	5
2.3	Dark matter sector	6
3	Phenomenology	7
3.1	Neutrino masses and mixing	7
3.2	Dark matter phenomenology	9
3.3	The anomalous magnetic moment of muon	10
4	Numerical results	10
5	Conclusion and discussion	13

1 Introduction

The Standard Model (SM) has been a cornerstone in understanding elementary particles and their interactions. Despite its successes, certain phenomena remain unexplained, notably the non-zero masses of neutrinos and the existence of dark matter (DM). The SM's failure to accommodate these observations has driven significant efforts to extend it, leading to a range of proposed mechanisms and models.

One of the most profound issues with the SM is its prediction of massless neutrinos. However, experimental evidence from Super-Kamiokande [1], SNO [2], KamLAND [3], Daya Bay [4], RENO[5], CHOOZ [6], K2K [7], T2K[8], and LSND [9] confirms that neutrinos undergo flavor oscillations, and hence are massive. Traditional seesaw mechanisms have been proposed to explain the smallness of neutrino masses by introducing heavy right-handed Majorana neutrinos, which generate light neutrino masses suppressed by the heavy Majorana scale [10–15], commonly referred to as the seesaw scale. However, the traditional seesaw mechanism usually requires a seesaw scale around $M \sim 10^{12}$ GeV, which greatly reduces the possibility to probe the model experimentally. On the other hand, the inverse seesaw model [16–22] offers a more testable neutrino mass generation mechanism. In this scenario, sterile neutrinos with small, yet technically natural, lepton number-violation (LNV) couplings are introduced. These small LNV couplings help to lower the seesaw scale down to within reach of colliders. This approach has gained traction as a realistic and testable framework, with studies exploring its implications on lepton flavor violation (LFV) and collider phenomenology [17, 23–30].

On the other hand, the existence of DM has been firmly established through astrophysical observations, such as galaxy rotation curves [31, 32] and cosmic microwave background measurements [33–35]. Various extensions of the SM have been proposed to accommodate DM, see Ref. [36–41] for recent reviews. One of the most studied scenario is the Higgs portal DM [42], thanks to its simplicity and predictive nature. In this framework, the Higgs boson serves as a mediator between the DM and the SM sector. Phenomenology of the Higgs portal DM has been studied in Ref. [43–45]. Due to its minimal structure, the Higgs portal model cannot accommodate neutrino masses without a further extension.

An alternative and compelling approach is the axion portal model, which introduces an axion or axion-like particle (ALP) as a mediator between the DM and the SM sectors. Initially proposed to address the strong CP problem in quantum chromodynamics, axion has gained interest in DM studies due to their weak interactions and stability [46–48]. ALP portal models offers unique signatures in indirect detection experiment, cosmic microwave background distortions, and low energy precision measurements, which can differentiate them from Higgs portal models [49–52]. It is also interesting to note that ALP can be connected to neutrino mass generation models as well [53].

Another intriguing anomaly is the muon anomalous magnetic moment, $g - 2$, where current experimental measurements at Fermilab [54, 55] and previous measurements at Brookhaven National Laboratory [56] exceed the SM prediction [57]. This discrepancy, standing at about 5σ , suggests possible contributions from physics beyond the SM.¹ Various models, including those with extended Higgs sectors [61–63], sterile neutrinos [64, 65], or new gauge bosons [66, 67], attempt to account for this deviation by introducing additional contributions to $g - 2$. In particular, models involving dark sectors or ALPs have been investigated for their potential to explain the muon $g - 2$ anomaly [68–71].

In this work, we build upon these developments by proposing a minimal SM extension that combines the inverse seesaw mechanism for neutrino mass generation and the ALP portal DM. Our model draws from the previous study that explored Higgs portals in the DM-neutrino mass model [72], aiming instead to utilize the ALP portal [71, 73–82], which offers new dynamics and observables. In this work, we also attempt to explain the muon $g - 2$ anomaly within the ALP portal model, which place a non-trivial constraint on the model parameter space. This approach not only addresses the neutrino mass and DM issues within a unified framework but also proposes testable signatures that could guide future experimental searches.

The paper is organised as follows. The model and particle contents are discussed in detail in section 2. In section 3, we discuss the model phenomenology and relevant constraints. Numerical results are presented in section 4. Finally, we summarise our findings and express an outlook in section 5.

¹The recent lattice simulation [58] and experimental results [59, 60] have called into question the validity of the SM prediction.

2 The model

In this work, we propose an extension to the SM with an electroweak (EW) singlet complex scalar (Φ), two EW singlet right-handed heavy neutrinos (N_R^i), two EW singlet left-handed heavy neutrinos (S_L^i), and a pair of fermionic dark matter (χ_L and χ_R).² In addition, the $U(1)_{PQ}$ global symmetry is imposed to stabilise the DM sector, and is assumed to be broken at a scale higher than the EW symmetry breaking scale. The relevant particle contents and their charge assignment under $SU(2)_L \times U(1)_Y \times U(1)_{PQ}$ is summarised in Tab. 1.

	$SU(2)_L$	$U(1)_Y$	$U(1)_{PQ}$
L	2	$-1/2$	X_N
H	2	$+1/2$	0
N_R	1	0	X_N
S_L	1	0	$X_N + 1$
χ_R	1	0	X_χ
χ_L	1	0	$X_\chi + 1$
Φ	1	0	1

Table 1: The charge assignment under the electroweak and $U(1)_{PQ}$ groups.

2.1 The scalar sector

The scalar potential consistent with $U(1)_{PQ}$ is given by

$$V(H, \Phi) = -\mu_H^2 H^\dagger H + \lambda_H (H^\dagger H)^2 - \mu_\Phi^2 \Phi^\dagger \Phi + \lambda_\Phi (\Phi^\dagger \Phi)^2 + \lambda_{H\Phi} (H^\dagger H) (\Phi^\dagger \Phi). \quad (2.1)$$

The field H and Φ can be expanded as

$$H = \frac{1}{\sqrt{2}} \begin{pmatrix} \sqrt{2}G^+ \\ v_h + h' + iG^0 \end{pmatrix}, \quad \Phi = \frac{1}{\sqrt{2}} (v_\phi + \phi') e^{ia/f_a}, \quad (2.2)$$

where G^+ and G^0 are the would-be Goldstone boson. v_h , v_ϕ and f_a are the vacuum expectation values (vev) of H and Φ and the ALP decay constant, respectively. Since $U(1)_{PQ}$ is assumed to be broken at scale higher than the EW scale, we have $v_\phi, f_a > v_h$. Note that we employ the non-linear parametrization for Φ which makes the ALP, a , appears explicitly as the phase. The fields h' and ϕ' mix to form the mass eigenstates

$$\begin{pmatrix} h \\ \phi \end{pmatrix} = \begin{pmatrix} \cos \theta & \sin \theta \\ -\sin \theta & \cos \theta \end{pmatrix} \begin{pmatrix} h' \\ \phi' \end{pmatrix}, \quad (2.3)$$

²Scenarios with one N_R and one S_L , or one N_R and two S_L lead to two vanishing light neutrino masses. Scenario with two N_R and one S_L is compatible with neutrino oscillation data. However, it would require more free parameters than the scenario presented in this work.

where

$$\tan(2\theta) = \frac{\lambda_{H\Phi} v_h v_\phi}{\lambda_\Phi v_\phi^2 - \lambda_H v_h^2}. \quad (2.4)$$

Here we identify the field h with the 125 GeV Higgs boson. The masses of h and ϕ are given by

$$m_{h,\phi}^2 = \lambda_H v_h^2 + \lambda_\Phi v_\phi^2 \mp \sqrt{(\lambda_\Phi v_\phi^2 - \lambda_H v_h^2)^2 + \lambda_{H\Phi}^2 v_h^2 v_\phi^2}. \quad (2.5)$$

It is more convenient to express the quartic couplings λ_H , λ_Φ , and $\lambda_{H\Phi}$ in terms of the vevs, the masses and the mixing angle. They are given by

$$\begin{aligned} \lambda_H &= \frac{m_h^2 \cos^2 \theta + m_\phi^2 \sin^2 \theta}{v_h^2}, \\ \lambda_\Phi &= \frac{m_h^2 \sin^2 \theta + m_\phi^2 \cos^2 \theta}{v_\phi^2}, \\ \lambda_{H\Phi} &= \frac{(m_\phi^2 - m_h^2) \sin \theta \cos \theta}{v_h v_\phi}. \end{aligned} \quad (2.6)$$

Thus, the scalar potential can be described by three free parameters: v_ϕ , m_ϕ and $\sin \theta$. We note that $\sin \theta$ is constrained by the 125 GeV Higgs boson measurement. The latest results from the ATLAS and CMS collaborations place an upper bound on $\sin \theta \leq 0.12$ [83, 84].

The ALP potential, on the other hand, is generated from the non-perturbative effect, which breaks $U(1)_{PQ}$ into a shift symmetry, $a \rightarrow a + f_a$. This shift symmetry dictates that the ALP potential takes the form of the instanton cosine potential [85]

$$V(a) = \tilde{\Lambda}_a^4 \left[1 - \cos \left(\frac{2\pi a}{f_a} \right) \right], \quad (2.7)$$

where $\tilde{\Lambda}_a^4$ is the maximum value of the potential. By identifying this shift under $U(1)_{PQ}$ transformation with the period of the ALP potential, one obtains a relation

$$f_a = v_\phi. \quad (2.8)$$

From now on we will use f_a in place of v_ϕ . The ALP potential also generates the ALP mass

$$m_a^2 = \frac{\Lambda_a^4}{f_a}, \quad (2.9)$$

where $\Lambda_a^2 \equiv 2\pi \tilde{\Lambda}_a^2$.

Below the $U(1)_{PQ}$ symmetry breaking scale, f_a , the interaction of ALP with other particles is given by the effective operators

$$\begin{aligned} \mathcal{L}_{\text{ALP}} &= \frac{C_{\psi\psi}}{f_a} (\partial_\mu a) \bar{\psi} \gamma^\mu \gamma_5 \psi + \frac{g_s^2}{16\pi^2} C_{gg} \frac{a}{f_a} G_{\mu\nu}^a \tilde{G}^{a\mu\nu} \\ &+ \frac{g^2}{16\pi^2} C_{WW} \frac{a}{f_a} W_{\mu\nu}^i \tilde{W}^{i\mu\nu} + \frac{g'^2}{16\pi^2} C_{BB} \frac{a}{f_a} B_{\mu\nu} \tilde{B}^{\mu\nu}, \end{aligned} \quad (2.10)$$

where ψ is the SM fermion with the ALP coupling $C_{\psi\psi}$. The couplings g_s , g , and g' are the strong, weak, and hypercharge gauge couplings respectively, and C_{VV} is the gauge-ALP coupling. The dual field strength tensor is defined as $\tilde{F}_{\mu\nu} = \frac{1}{2}\epsilon_{\mu\nu\alpha\beta}F^{\alpha\beta}$. The fields B and W_3 mix to become the photon and the Z -boson via

$$\begin{pmatrix} Z \\ A \end{pmatrix} = \begin{pmatrix} c_W & -s_W \\ s_W & c_W \end{pmatrix} \begin{pmatrix} W^3 \\ B \end{pmatrix}, \quad (2.11)$$

where s_W and c_W are the sine and cosine of the Weinberg angle respectively. We also define $W_\mu^\pm = (W_\mu^1 \mp iW_\mu^2)/\sqrt{2}$. Then, the gauge-ALP interaction can be recast into the form

$$\begin{aligned} \mathcal{L}_{\text{gauge-ALP}} = & C_{\gamma\gamma} \frac{\alpha}{4\pi} \frac{a}{f_a} F\tilde{F} + C_{ZZ} \frac{\alpha}{4\pi s_W^2 c_W^2} \frac{a}{f_a} Z\tilde{Z} \\ & + \left(C_{WW} \frac{\alpha}{4\pi s_W^2} \frac{a}{f_a} W\tilde{W} + C_{\gamma Z} \frac{\alpha}{4\pi s_W c_W} \frac{a}{f_a} A\tilde{Z} + \text{h.c.} \right), \end{aligned} \quad (2.12)$$

where we introduce a shorthand notation $F\tilde{F} = F_{\mu\nu}\tilde{F}^{\mu\nu}$, $\alpha = e^2/4\pi$ is the fine structure constant, and

$$C_{\gamma\gamma} = C_{WW} + C_{BB}, \quad C_{\gamma Z} = c_W^2 C_{WW} - s_W^2 C_{BB}, \quad C_{ZZ} = c_W^4 C_{WW} + s_W^4 C_{BB}. \quad (2.13)$$

2.2 The neutrino sector

In this section, we derive the light neutrino mass matrix in the inverse seesaw scenario. The Yukawa interactions consistent with the global $U(1)_{PQ}$ are given by

$$\mathcal{L}_{Yuk} \supset -Y^{\alpha i} \bar{L}^\alpha \tilde{H} N_R^i - Y^{Ii} \Phi \bar{S}_L^I N_R^i + \text{h.c.}, \quad (2.14)$$

where α , i , and I are generation indices, and $\tilde{H} = i\sigma_2 H^*$. These interactions by themselves do not violate lepton number, and hence cannot generate neutrino mass. Thus, we also introduce the LNV Majorana mass terms

$$\mathcal{L}_{Maj.} = -\frac{\mu_R^{ij}}{2} \bar{N}_R^c N_R^j - \frac{\mu_S^{IJ}}{2} \bar{S}_L^I S_L^J + \text{h.c.}, \quad (2.15)$$

where $\psi^c = C\bar{\psi}^T$ is the charge conjugated field. The μ_R and μ_S terms also break $U(1)_{PQ}$ softly. However, they are expected to be small thanks to 't Hooft technical naturalness argument. After $U(1)_{PQ}$ and EW symmetry breaking, Eq. (2.14) and (2.15) lead to the neutrino mass terms

$$\begin{aligned} -\mathcal{L}_{\text{mass}}^\nu = & m_D^{\alpha i} \bar{\nu}^\alpha N_R^i + M_N^{Ij} \bar{S}_L^I N_R^j \\ & + \frac{\mu_R^{ij}}{2} \bar{N}_R^c N_R^j + \frac{\mu_S^{IJ}}{2} \bar{S}_L^I S_L^J + \text{h.c.}, \end{aligned} \quad (2.16)$$

where we define $m_D^{\alpha i} = Y^{\alpha i} v_h / \sqrt{2}$ and $M_N^{Ij} = Y^{Ij} f_a / \sqrt{2}$. The neutrino mass terms can be written in a compact form

$$-\mathcal{L}_{\text{mass}}^\nu = \frac{1}{2} \overline{\psi_R^c} \mathcal{M}_\nu \psi_R + \text{h.c.}, \quad (2.17)$$

where

$$\psi_R = \begin{pmatrix} \nu_L^c \\ N_R \\ S_L^c \end{pmatrix}, \quad \mathcal{M}_\nu = \begin{pmatrix} \mathbf{0} & m_D & \mathbf{0} \\ m_D^T & \mu_R & M_N^T \\ \mathbf{0} & M_N & \mu_S \end{pmatrix}. \quad (2.18)$$

The neutrino mass matrix \mathcal{M}_ν can be brought to a block diagonal form by [15]

$$V^T \mathcal{M}_\nu V = \begin{pmatrix} (M_{\text{light}})_{3 \times 3} & \mathbf{0} \\ \mathbf{0} & (M_{\text{heavy}})_{4 \times 4} \end{pmatrix}, \quad (2.19)$$

where V is a unitary matrix, M_{light} and M_{heavy} are the light neutrino and heavy neutrino mass matrices respectively. In the limit where $\|\mu_R\|, \|\mu_S\| \ll \|m_D\| \ll \|M_N\|$ ³, M_{light} can be approximated by

$$M_{\text{light}} \simeq -m_D M_N^{-1} \mu_S (M_N^T)^{-1} m_D^T. \quad (2.20)$$

Note that, to lowest order, the Majorana mass term μ_R does not contribute to M_{light} . Notice also that in this case, M_{light} receives an extra suppression of order $\|\mu_S\|/\|M_N\|$ compared to the usual seesaw scenario. This makes it possible to place a seesaw scale within reach of collider experiment.

2.3 Dark matter sector

The dynamics of the DM sector is governed by the Yukawa interaction

$$\mathcal{L}_{DM} = -g_\chi \Phi \overline{\chi} \chi_R + \text{h.c.} \quad (2.21)$$

The $U(1)_{PQ}$ symmetry breaking generates a DM mass, $m_\chi = g_\chi f_a / \sqrt{2}$. Below the $U(1)_{PQ}$ breaking scale, DM interactions are given by

$$\begin{aligned} \mathcal{L}_{DM} \supset & -\frac{m_\chi}{f_a} \sin \theta h \overline{\chi} \chi - \frac{m_\chi}{f_a} \cos \theta \phi \overline{\chi} \chi - i \frac{m_\chi}{f_a} a \overline{\chi} \gamma_5 \chi \\ & - i \frac{g_\chi \cos \theta}{\sqrt{2} f_a} a \phi \overline{\chi} \chi - i \frac{g_\chi \sin \theta}{\sqrt{2} f_a} a h \overline{\chi} \chi, \end{aligned} \quad (2.22)$$

where θ is the neutral scalars mixing angle defined in Eq. (2.4).

From the above interaction, one sees that the h , ϕ and a can serve as a portal between the DM sector and the SM sector. However, the h and ϕ portal to SM fermions and gauge bosons are suppressed by $\sin^2 2\theta \lesssim 0.06$ due to the mixing in the neutral scalar sector. The ALP portal, on the other hand, does not suffer from this suppression. For simplicity, we will assume $\theta = 0$ in this work. Thus, DM phenomenology is mediated by the ALP portal.

³Here we define $\|M\| \equiv \sqrt{\text{Tr}(M^\dagger M)}$.

3 Phenomenology

In this section, we study the phenomenology of our model. We are interested in the minimal scenario, in the sense of the least number of free parameters, which could explain 1) neutrino masses and mixing, 2) dark matter relic density, and 3) the muon $g-2$ anomaly.

3.1 Neutrino masses and mixing

In our scenario m_D is a complex 3×2 matrix, M_N is a complex 2×2 matrix and μ_S is a symmetric complex 2×2 matrix. However, not all components of these matrices are physical. One can perform unitary field redefinitions on N_R^i and S_L^I to put M_N and μ_S in the form

$$m_N \sim \text{diag.}(1, \gamma), \quad (3.1)$$

$$\mu_S \sim \begin{pmatrix} 1 & \alpha\gamma \\ \alpha\gamma & \beta\gamma^2 e^{i\phi} \end{pmatrix}, \quad (3.2)$$

where γ , α , β and ϕ are real and positive. Note that our parametrization of m_N and μ_S makes explicit that γ drops out from the light neutrino mass matrix. In the above equations, we have also factored out the 1-1 components from both m_N and μ_S . Moreover, by redefining the phases of L^α and N^i , one can rotate away 4 phases in m_D . From our analysis, we find two minimal textures of m_D , which lead to viable neutrino masses and mixing. They are

$$m_D^{(A)} \sim \begin{pmatrix} 1 & 0 \\ y_1 & y_2 \\ 0 & y_3 \end{pmatrix}, \quad (3.3)$$

$$m_D^{(B)} \sim \begin{pmatrix} 1 & 0 \\ 0 & y_1 \\ y_2 & y_3 \end{pmatrix}, \quad (3.4)$$

where $y_i > 0$. Again, we have factored out the 1-1 component of m_D . Finally, the light neutrino mass matrix are given by

$$M_{\text{light}}^{(A)} = \kappa \begin{pmatrix} 1 & y_1 + \alpha y_2 & \alpha y_3 \\ y_1 + \alpha y_2 & y_1^2 + 2\alpha y_1 y_2 + \beta e^{i\phi} y_2^2 & \alpha y_1 y_3 + \beta e^{i\phi} y_2 y_3 \\ \alpha y_3 & \alpha y_1 y_3 + \beta e^{i\phi} y_2 y_3 & \beta e^{i\phi} y_3^2 \end{pmatrix}, \quad (3.5)$$

$$M_{\text{light}}^{(B)} = \kappa \begin{pmatrix} 1 & \alpha y_1 & y_2 + \alpha y_3 \\ \alpha y_1 & \beta e^{i\phi} y_1^2 & \alpha y_1 y_2 + \beta e^{i\phi} y_1 y_3 \\ y_2 + \alpha y_3 & \alpha y_1 y_2 + \beta e^{i\phi} y_1 y_3 & y_2^2 + 2\alpha y_2 y_3 + \beta e^{i\phi} y_3^2 \end{pmatrix}, \quad (3.6)$$

where $\kappa \sim v^2 ||\mu_S||/f_a^2$ is the overall scale of neutrino masses. Thus, in our scenario, M_{light} depends on 7 real parameters: κ , $y_{1,2,3}$, a , b , and ϕ .

Parameters	Normal Ordering	Inverted Ordering
$\sin^2 \theta_{12}$	$0.308^{+0.037}_{-0.033}$	$0.308^{+0.037}_{-0.033}$
$\sin^2 \theta_{13}$	$0.02215^{+0.00173}_{-0.00185}$	$0.02231^{+0.00178}_{-0.00171}$
$\sin^2 \theta_{23}$	$0.470^{+0.115}_{-0.035}$	$0.550^{+0.034}_{-0.110}$
$m_{\text{solar}}^2/10^{-5} \text{ eV}^{-2}$	$7.49^{+0.56}_{-0.57}$	$7.49^{+0.56}_{-0.57}$
$m_{\text{atm}}^2/10^{-3} \text{ eV}^{-2}$	$2.513^{+0.065}_{-0.062}$	$2.484^{+0.063}_{-0.063}$
$\delta_{\text{CP}}/^\circ$	212^{+152}_{-88}	274^{+61}_{-73}

Table 2: The best fit values of neutrino oscillation parameters and their 3σ ranges as determined from the global neutrino data [86]. Here $m_{\text{solar}}^2 = m_2^2 - m_1^2$ and $m_{\text{atm}}^2 = m_3^2 - m_1^2$ ($m_2^2 - m_3^2$) for normal ordering (inverted ordering).

The light neutrino mass matrix can be diagonalized by a unitary matrix U ,

$$U^T M_{\text{light}} U = \text{diag.}(m_1, m_2, m_3), \quad (3.7)$$

where $m_i > 0$ are the mass eigenvalues. The above equation defines the Pontecorvo–Maki–Nakagawa–Sakata (PMNS) matrix. In general, the PMNS matrix contains three mixing angles, one Dirac phase, and two Majorana phases.

Once the neutrino mass matrix M_{light} has been diagonalized, the three mixing angles can be determined by

$$s_{13}^2 = |U_{e3}|^2, \quad s_{12}^2 = \frac{|U_{e2}|^2}{1 - |U_{e3}|^2}, \quad s_{23}^2 = \frac{|U_{\mu 3}|^2}{1 - |U_{e3}|^2}, \quad (3.8)$$

where $s_{ij} = \sin \theta_{ij}$ is the sine of the mixing angles. The Dirac phase, δ_{CP} , is encoded in the Jarshklog invariant

$$J = \text{Im} (U_{\mu 3} U_{e3}^* U_{e2} U_{\mu 2}^*). \quad (3.9)$$

The remaining two Majorana phases, in principle, can be deduced from the invariants $\text{Im}[(U_{e2} U_{e1}^*)^2]$ and $\text{Im}[(U_{e3} U_{e1}^*)^2]$ [87]. However, both Majorana phases have never been determined experimentally. The values of neutrino masses, mixing angles, and the Dirac phase, as determined from the global analysis of neutrino data, are collected in Tab. 2.

An interesting feature of our set up is that the light neutrino mass matrix is rank 2. As a result, the lightest neutrino mass is vanishing. Hence, the other two non vanishing neutrino masses depend only on Δm_{sol}^2 and Δm_{atm}^2 . In particular, the sum of neutrino masses is given by $\sum_i m_i = \sqrt{\Delta m_{\text{sol}}^2} + \sqrt{\Delta m_{\text{atm}}^2}$ and $\sqrt{\Delta m_{\text{atm}}^2 - \Delta m_{\text{sol}}^2} + \sqrt{\Delta m_{\text{atm}}^2}$ for the NO and IO scenarios respectively. The sum of neutrino masses is constrained by cosmological measurement. Combining the Planck 2018 cosmic microwave background data and the baryonic acoustic oscillation measurement result in an upper bound $\sum_i m_i \leq 130 \text{ meV}$ at 95% confidence level (CL) [33]. In addition to the neutrino masses sum, there are two effective masses relevant for laboratory based neutrino experiments. First, the effective mass $m_{\nu_e}^{\text{eff}} = \sqrt{\sum_i |U_{ei}|^2 m_i^2}$ determines the endpoint of beta decay spectrum. The latest

measurement published by KATRIN has put an upper bound of $m_{\nu_e}^{\text{eff}} \leq 450$ meV at 90% CL [88]. Second the rate for neutrinoless double beta ($0\nu\beta\beta$) decay depends on the effective mass $m_{ee} = |\sum_i U_{ei}^2 m_i|$. The strongest upper bound on m_{ee} is provided by the KamLAND-Zen experiment with $m_{ee} \leq 36 - 156$ meV at 90% CL [89].

3.2 Dark matter phenomenology

In addition to generating neutrino masses, our model also provides a DM candidate which is assumed to be a fermion, χ . In the absence of the neutral scalar mixing, θ , DM interaction with the SM sector is mediated by the ALP, see Eq. (2.22). Moreover, in the spirit of minimality, the ALP is taken to couple only to muons and photons to explain the muon $g - 2$ anomaly, see Sec. 3.3. As a result, assuming ϕ and a are heavier than χ , there are only two DM annihilation channels

$$\sigma_{\gamma\gamma} v_{\text{rel}} \simeq \frac{1}{4\pi^3} \frac{\alpha^2 C_{\gamma\gamma}^2 m_\chi^6}{(m_a^2 - 4m_\chi^2)^2 f_a^4}, \quad (3.10)$$

$$\sigma_{\mu\bar{\mu}} v_{\text{rel}} \simeq \frac{8}{\pi} \frac{C_{\mu\mu}^2 m_\mu^2 m_\chi^4}{(m_a^2 - 4m_\chi^2)^2 f_a^4} \sqrt{1 - \frac{4m_\mu^2}{m_\chi^2}}, \quad (3.11)$$

where m_μ is the mass of the muon. Note that the $\mu\bar{\mu}$ annihilation channel is parametrically suppressed by

$$\frac{\sigma_{\mu\bar{\mu}}}{\sigma_{\gamma\gamma}} \sim \frac{\pi^2 C_{\mu\mu}^2 m_\mu^2}{\alpha^2 C_{\gamma\gamma}^2 m_\chi^2}. \quad (3.12)$$

Thus, for $m_\chi \gtrsim 1$ TeV, one expects the $\mu\bar{\mu}$ channel to be irrelevant unless there is a large hierarchy in $C_{\mu\mu}$ and $C_{\gamma\gamma}$.

The energy density of DM is precisely measured by the Planck satellite [33] to be

$$\Omega_{\text{DM}}^{\text{Planck}} h^2 = 0.12 \pm 0.0012. \quad (3.13)$$

Assuming DM is present in the thermal bath of the early Universe, its present energy density is related to its annihilation cross section. The value of DM energy density can be determined by solving Boltzman equation numerically. However, here we will adopt a simple freeze out approximation, which yields the thermal relic cross section $\langle\sigma v_{\text{rel}}\rangle = 2.6 \times 10^{-26}$ cm³/s. In our numerical analysis, we take $\pm 0.4 \times 10^{-26}$ cm³/s as the nominal error associate with the approximation. The thermal relic cross section, in turns, constrains the possible range of the ALP couplings $C_{\gamma\gamma}$ and $C_{\mu\bar{\mu}}$. In our numerical analysis, we also verify that the our results based on the freeze out approximation are consistent with MICROMEGAS [90, 91]. To this end, we have implemented the model files in LAMHEP [92], and then feed them to CALCHEP [93] and MICROMEGAS for numerical computation.

The DM annihilation cross sections in Eqs. (3.10) and (3.11) also give rise to detectable signals in gamma ray telescopes. The annihilation channel $\sigma_{\gamma\gamma} v_{\text{rel}}$ leads to a line signal in gamma ray spectrum at energy equals to DM mass. Such a signal has been searched for at the FermiLAT telescope in the low DM mass range, $m_\chi \lesssim 1$ TeV [94]. The heavier DM mass range, $m_\chi \leq 100$ TeV, has been searched for by H.E.S.S. [95] and MAGIC [96].

3.3 The anomalous magnetic moment of muon

As mentioned before, this model has an ability to explain the muon $g - 2$ anomaly. Currently, the combination of BNAL and FNAL run 1-3 results in the discrepancy of [97]

$$\Delta a_\mu \equiv a_\mu^{\text{EXP}} - a_\mu^{\text{SM}} = (249 \pm 48) \times 10^{-11}, \quad (3.14)$$

where $a_\mu = (g - 2)/2$. The discrepancy stands at a 5σ level and invites new physics interpretation.

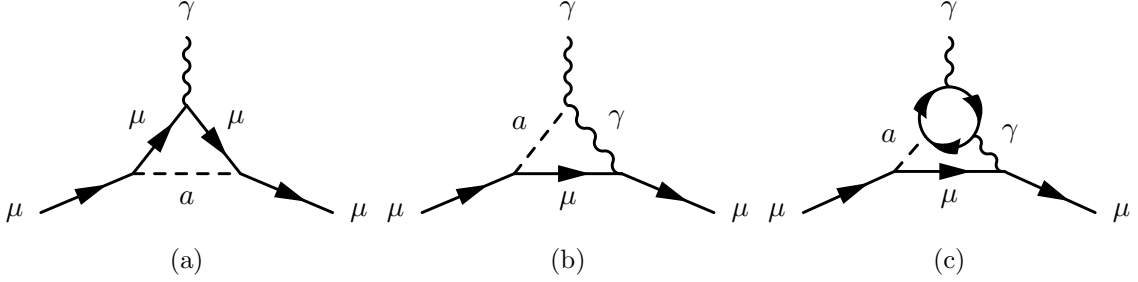


Figure 1: The representative diagrams for axion contribution to muon $g - 2$. The left and middle panels are one-loop contribution while the right is the two-loop one.

The new positive contributions to a_μ can be induced by the ALP-photon and ALP-muon couplings

$$\mathcal{L} \supset C_{\gamma\gamma} \frac{\alpha}{4\pi} \frac{a}{f_a} F_{\mu\nu} \tilde{F}^{\mu\nu} + \frac{C_{\mu\mu}}{f_a} (\partial_\mu a) \bar{\mu} \gamma^\mu \gamma_5 \mu,$$

through the Feynman diagrams shown in Fig. 1. The analytical result for each diagram is given by [68, 69]

$$\begin{aligned} \Delta a_\mu^{(a)} &= - \left(\frac{C_{\mu\mu}}{f_a} m_\mu \right)^2 \frac{1}{8\pi^2} \frac{m_\mu^2}{m_a^2} \int_0^1 dx \frac{x^3}{1 - x + m_\mu^2/m_a^2 x^2}, \\ \Delta a_\mu^{(b)} &= - \left(\frac{C_{\mu\mu}}{f_a} \right) \left(\frac{C_{\gamma\gamma}}{f_a} \right) \frac{\alpha}{4\pi^3} m_\mu^2 \int_0^1 dx \left[(1-x) \left(\log \left[\frac{4\pi f_a^2}{m_\mu^2 x^2 + m_a^2 (1-x)} \right] - \frac{1}{2} \right) \right. \\ &\quad \left. - \frac{3}{m_a^2/m_\mu^2} \left(x^2 \log \left[\frac{x^2 + m_a^2/m_\mu^2 (1-x)}{x^2} \right] \right) \right], \\ \Delta a_\mu^{(c)} &= \frac{\alpha}{8\pi^3} \left(\frac{C_{\mu\mu}}{f_a} \right)^2 m_\mu^2 \int_0^1 dx \frac{m_\mu^2}{m_\mu^2 + m_a^2 x(1-x)} \log \left[\frac{m_\mu^2}{m_a^2 x(1-x)} \right]. \end{aligned} \quad (3.15)$$

It should be noted that diagrams 1 (a) and (c) generate a negative and positive contribution to Δa_μ respectively. The contribution of diagram 1 (b) could be either positive or negative depending on the relative sign of $C_{\gamma\gamma}$ and $C_{\mu\mu}$.

4 Numerical results

In this section, we perform the numerical scan on the model parameter space. In our setup, the free parameters can be divided into two groups– neutrino, and DM and muon $g - 2$. We

first analyze the neutrino sector which depend on 7 free parameters. The free parameters are varied within the following ranges:

$$1 \text{ meV} \leq \kappa \leq 1 \text{ eV}, \quad 10^{-3} \leq y_i, a, b \leq 10^3, \quad 0 \leq \phi \leq 2\pi. \quad (4.1)$$

We search for the region of parameter space which is consistent with the neutrino oscillation data at the 3σ level. We then deduce the corresponding values for $\sum_i m_i$, $m_{\nu_e}^{\text{eff}}$, and m_{ee} .

Texture	δ_{CP} [°]	$\sum_i m_i$ [meV]	$m_{\nu_e}^{\text{eff}}$ [meV]	m_{ee} [meV]
A	124.16–289.95	58.09–59.21	8.64–9.00	1.16–3.04
B	124.18–289.93	58.25–59.20	8.69–9.14	1.85–4.01

Table 3: The range of δ_{CP} , $\sum m_i$, $m_{\nu_e}^{\text{eff}}$ and m_{ee} in each scenario.

We find both $m_D^{(A)}$ and $m_D^{(B)}$ can only accommodate NO neutrino masses. As a result, we have $\sum_i m_i = \sqrt{\Delta m_{\text{sol}}^2} + \sqrt{\Delta m_{\text{atm}}^2}$ and

$$\left(m_{\nu_e}^{\text{eff}}\right)^2 = s_{12}^2 c_{13}^2 \Delta m_{\text{sol}}^2 + s_{13}^2 \Delta m_{\text{atm}}^2. \quad (4.2)$$

Moreover, due to our parametrization of the M_{light} , we get $m_{ee} = \kappa$. The ranges of these masses consistent with neutrino oscillation data, are shown in Tab. 3. The values of these effective masses are well below their corresponding experimental bounds.

In our framework, the parameter ϕ is responsible for CP violation. We find a strong correlation between ϕ and the Dirac phase δ in both scenarios A and B, see Fig. 2 (a). We also observe an upper bound $\delta \lesssim 290^\circ$ in both scenarios. More interestingly, we have identified a strong correlation between m_{ee} and δ , see Fig. 2 (b). Their relationship can be well approximated by an empirical formula

$$m_{ee}^{(A)} = s_{12}^2 c_{13}^2 \sqrt{\Delta m_{\text{sol}}^2} + s_{13}^2 \sqrt{\Delta m_{\text{atm}}^2} \cos(\delta_{\text{CP}}), \quad (4.3)$$

$$m_{ee}^{(B)} = s_{12}^2 c_{13}^2 \sqrt{\Delta m_{\text{sol}}^2} + s_{13}^2 \sqrt{\Delta m_{\text{atm}}^2} \cos(\delta_{\text{CP}} + \pi). \quad (4.4)$$

For the DM and muon $g-2$ sector, there are 5 free parameters: m_χ , m_a , f_a , $C_{\gamma\gamma}$ and $C_{\mu\mu}$. Here, we identify the region of parameter space consistent with the observed DM relic abundance which can also explain the muon $g-2$ anomaly. We have also taken into account constraints from gamma ray line searches. We find that in our setup, we need a rather heavy f_a scale, $f_a \gtrsim 10$ TeV. Fig. 3 shows the allowed parameter space on the $m_a - C_{\gamma\gamma}/f_a$ plane for the benchmark scenario $m_a = m_\phi = 1.1m_\chi$ with $C_{\mu\mu}/f_a = -0.01, -0.1, -1$ [GeV $^{-1}$] and $f_a = 10, 100$ TeV respectively. The narrow sky blue region shows the parameter space consistent with DM relic density. The green, teal, and deep blue stripes represent the parameter space which can explain the muon $g-2$ anomaly for $C_{\mu\mu}/f_a = -0.01, -0.1$ and -1 [GeV $^{-1}$] respectively. The dotted gold region is ruled out by the overabundance of DM. The rose, coral, and orange hatched regions are ruled out by gamma ray line searches at FermiLAT [98], H.E.S.S. [95], and Magic [96] respectively. We have also included the

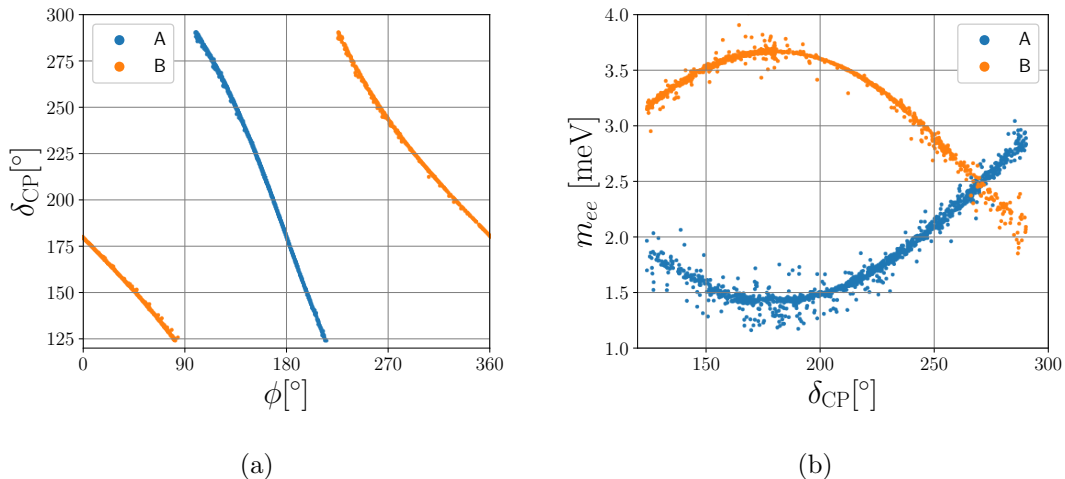


Figure 2: The relations between the free parameter ϕ and δ (a), and δ and m_{ee} (b) in scenarios A and B.

projected exclusion region of the upcoming Cherenkov Telescope Array (CTA) [99] which is shown in the crimson hatched region.

In the case of $f_a = 10$ TeV, we find that only $C_{\mu\mu}/f_a = -1$ [GeV $^{-1}$] can reproduce the DM density and explain the muon $g - 2$ anomaly while remaining consistent with the current gamma ray line searches. However, this scenario would be probed by the upcoming CTA. On the other hand, when $f_a = 100$ TeV, all $C_{\mu\mu}/f_a = -0.01$, -0.1 and -1 can provide the solutions to $g - 2$ anomaly and being consistent with DM relic density and gamma ray line constraints. Unfortunately, these scenarios lie beyond the reach of CTA.

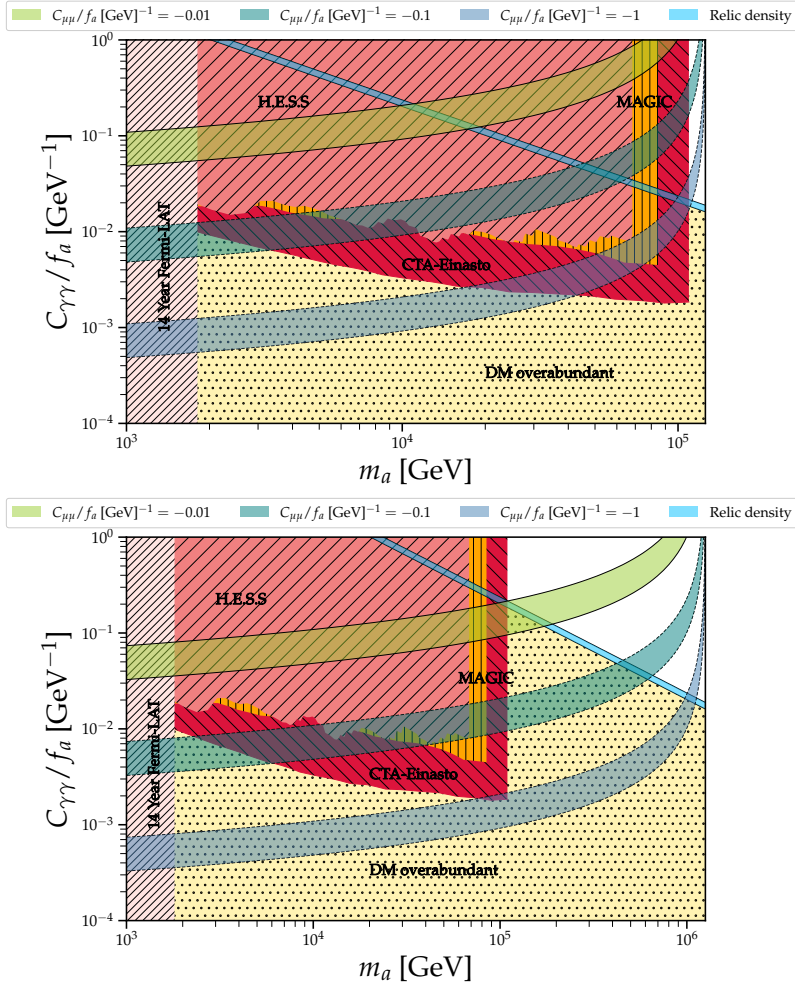


Figure 3: The region of parameter space on the $m_a - C_{\gamma\gamma}/f_a$ plane consistent with the DM relic density (sky blue) and can explain the muon $g - 2$ anomaly (green, teal and deep blue for $C_{\mu\mu}/f_a = -0.01, -0.1$ and -1 [GeV^{-1}] respectively). In these plots, $m_a = m_\phi = 1.1m_\chi$. The hatched region is ruled out by the gamma ray line search and the dotted region produces an over abundance of DM. In the top (bottom) figure, $f_a = 10$ (100) TeV.

5 Conclusion and discussion

We presented a minimal extension of the SM that combines the inverse seesaw mechanism with an ALP portal DM. This model addresses both the origin of neutrino masses and the nature of DM while remaining consistent with current experimental constraints. Unlike traditional seesaw models that require high mass scales, the inverse seesaw mechanism allows for TeV-scale new physics, making it potentially accessible in future collider experiments. Additionally, the ALP serves as a mediator between the SM and DM sectors, providing a distinct phenomenology that includes a positive contribution to the muon anomalous magnetic moment ($g - 2$) and compatibility with observed relic density.

From our analysis, we find two minimal scenarios for the inverse seesaw mechanism. They both lead to NO neutrinos with vanishing lightest neutrino mass. As a result, the total neutrino mass $\sum_i m_i$ and the effective masses $m_{\nu_e}^{eff}$ and m_{ee} are directly related to Δm_{sol}^2 and Δm_{atm}^2 . For the total neutrino mass, we find $\sum_i m_i \simeq 58$ meV. This is an order of magnitude below the current Planck constraint. However, it can be probed by the Simon Observatory whose projected sensitivity is $\sum_i m_i \leq 40$ meV at 95% CL [100]. Meanwhile, the effective mass $m_{\nu_e}^{eff}$ in our scenarios are around 9 meV, which is an order of magnitude below the projection $m_{\nu_e}^{eff} \leq 200$ meV at 90% CL of both the HOLMES and the KATRIN experiments [101, 102]. Moreover, we find the effective mass m_{ee} is of order a few meV. This is well below the projected sensitivity of $m_{ee} \leq 13 - 29$ meV at 90% CL of the LEGEND experiment phase II [103]. Thus, the key signature for our neutrino sector is a signal in cosmological measurements ($\sum_i m_i$) without corresponding signals in laboratory based measurements ($m_{\nu_e}^{eff}$ and m_{ee}).

In our scenario, the DM density is determined from the annihilation $\chi\bar{\chi} \rightarrow \gamma\gamma, \mu\bar{\mu}$ through a s-channel ALP exchange. For sufficiently large m_χ , the diphoton annihilation channel is expected to dominate over the dimuon channel. As a result, the parameter space is tightly constrained by the gamma ray line searches at gamma ray telescopes. In the benchmark scenario where $m_a = m_\phi = 1.1m_\chi$, we find that DM can be a thermal relic for $m_a \gtrsim 80$ TeV, see Fig. 3. The ALP couplings that determine DM density also generate a positive shift in the muon $g - 2$. We identify the region of parameter space in the $m_a - C_{\gamma\gamma}/f_a$ plane which could explain the muon $g - 2$ anomaly for $C_{\mu\mu}/f_a = -0.01, -0.1, -1$ [GeV⁻¹] respectively. Most of these parameter space regions are incompatible with DM being a thermal relic and/or the constraints from gamma ray line searches. In the case where $f_a = 10$ TeV, only the scenario where $C_{\mu\mu}/f_a = -1$ [GeV⁻¹] can satisfy both constraints for $m_a \sim 100$ TeV. This scenario can be probed by the upcoming CTA. In the case $f_a = 100$ TeV, all $C_{\mu\mu}/f_a = -0.01, -0.1, -1$ [GeV⁻¹] can satisfy both DM relic density and gamma ray line search constraints. Unlike the $f_a = 10$ TeV case, these region are out of reach of the CTA.

In our setup, we need $f_a \gtrsim 10$ TeV and $m_a \gtrsim 100$ TeV to be able to explain both the DM relic density and the muon $g - 2$ anomaly. This would put both scalars a and ϕ out of reach of the LHC and possibly the planned 100 TeV collider as well. The heavy neutrinos, on the other hand, can be at the scale f_a . Thus, in principle, they could be probed at the proposed 100 TeV collider such as the Future Circular Collider [104].

Acknowledgement

This research has received funding support from the NSRF via the Program Management Unit for Human Resources & Institutional Development, Research and Innovation [grant number B13F670063]. CP is supported by Fundamental Fund 2567 of Khon Kaen University via the National Science Research and Innovation Fund (NSRF). The work of PU is supported in part by the Mid-Career Research Grant from the National Research Council of Thailand under contract no. N42A650378. PU also thanks the High-Energy Physics

Research Unit, Chulalongkorn University for hospitality while part of this work was being completed.

References

- [1] Y. Fukuda et al. Evidence for oscillation of atmospheric neutrinos. *Phys. Rev. Lett.*, 81: 1562–1567, 1998. doi: 10.1103/PhysRevLett.81.1562.
- [2] Q. R. Ahmad et al. Direct evidence for neutrino flavor transformation from neutral current interactions in the Sudbury Neutrino Observatory. *Phys. Rev. Lett.*, 89:011301, 2002. doi: 10.1103/PhysRevLett.89.011301.
- [3] K. Eguchi et al. First results from KamLAND: Evidence for reactor anti-neutrino disappearance. *Phys. Rev. Lett.*, 90:021802, 2003. doi: 10.1103/PhysRevLett.90.021802.
- [4] F. P. An et al. Measurement of Electron Antineutrino Oscillation Amplitude and Frequency via Neutron Capture on Hydrogen at Daya Bay. *Phys. Rev. Lett.*, 133(15):151801, 2024. doi: 10.1103/PhysRevLett.133.151801.
- [5] J. K. Ahn et al. Observation of Reactor Electron Antineutrino Disappearance in the RENO Experiment. *Phys. Rev. Lett.*, 108:191802, 2012. doi: 10.1103/PhysRevLett.108.191802.
- [6] M. Apollonio et al. Limits on neutrino oscillations from the CHOOZ experiment. *Phys. Lett. B*, 466:415–430, 1999. doi: 10.1016/S0370-2693(99)01072-2.
- [7] M. H. Ahn et al. Indications of neutrino oscillation in a 250 km long baseline experiment. *Phys. Rev. Lett.*, 90:041801, 2003. doi: 10.1103/PhysRevLett.90.041801.
- [8] K. Abe et al. Indication of Electron Neutrino Appearance from an Accelerator-produced Off-axis Muon Neutrino Beam. *Phys. Rev. Lett.*, 107:041801, 2011. doi: 10.1103/PhysRevLett.107.041801.
- [9] A. Aguilar et al. Evidence for neutrino oscillations from the observation of $\bar{\nu}_e$ appearance in a $\bar{\nu}_\mu$ beam. *Phys. Rev. D*, 64:112007, 2001. doi: 10.1103/PhysRevD.64.112007.
- [10] Steven Weinberg. Baryon and Lepton Nonconserving Processes. *Phys. Rev. Lett.*, 43: 1566–1570, 1979. doi: 10.1103/PhysRevLett.43.1566.
- [11] Rabindra N. Mohapatra and Goran Senjanovic. Neutrino Mass and Spontaneous Parity Nonconservation. *Phys. Rev. Lett.*, 44:912, 1980. doi: 10.1103/PhysRevLett.44.912.
- [12] J. Schechter and J. W. F. Valle. Neutrino Masses in SU(2) x U(1) Theories. *Phys. Rev. D*, 22:2227, 1980. doi: 10.1103/PhysRevD.22.2227.
- [13] S. F. King. Neutrino mass models. *Rept. Prog. Phys.*, 67:107–158, 2004. doi: 10.1088/0034-4885/67/2/R01.
- [14] R. N. Mohapatra and J. W. F. Valle. Neutrino Mass and Baryon Number Nonconservation in Superstring Models. *Phys. Rev. D*, 34:1642, 1986. doi: 10.1103/PhysRevD.34.1642.
- [15] P. S. Bhupal Dev and Apostolos Pilaftsis. Minimal Radiative Neutrino Mass Mechanism for Inverse Seesaw Models. *Phys. Rev. D*, 86:113001, 2012. doi: 10.1103/PhysRevD.86.113001.
- [16] Stephen F. King and Christoph Luhn. Neutrino Mass and Mixing with Discrete Symmetry. *Rept. Prog. Phys.*, 76:056201, 2013. doi: 10.1088/0034-4885/76/5/056201.
- [17] Frank F. Deppisch, P. S. Bhupal Dev, and Apostolos Pilaftsis. Neutrinos and Collider Physics. *New J. Phys.*, 17(7):075019, 2015. doi: 10.1088/1367-2630/17/7/075019.

- [18] M. B. Gavela, T. Hambye, D. Hernandez, and P. Hernandez. Minimal Flavour Seesaw Models. *JHEP*, 09:038, 2009. doi: 10.1088/1126-6708/2009/09/038.
- [19] A. Ibarra, E. Molinaro, and S. T. Petcov. TeV Scale See-Saw Mechanisms of Neutrino Mass Generation, the Majorana Nature of the Heavy Singlet Neutrinos and $(\beta\beta)_{0\nu}$ -Decay. *JHEP*, 09:108, 2010. doi: 10.1007/JHEP09(2010)108.
- [20] F. Deppisch and J. W. F. Valle. Enhanced lepton flavor violation in the supersymmetric inverse seesaw model. *Phys. Rev. D*, 72:036001, 2005. doi: 10.1103/PhysRevD.72.036001.
- [21] P. S. Bhupal Dev and R. N. Mohapatra. TeV Scale Inverse Seesaw in SO(10) and Leptonic Non-Unitarity Effects. *Phys. Rev. D*, 81:013001, 2010. doi: 10.1103/PhysRevD.81.013001.
- [22] Arindam Das and Nobuchika Okada. Inverse seesaw neutrino signatures at the LHC and ILC. *Phys. Rev. D*, 88:113001, 2013. doi: 10.1103/PhysRevD.88.113001.
- [23] Paul Langacker. Grand Unified Theories and Proton Decay. *Phys. Rept.*, 72:185, 1981. doi: 10.1016/0370-1573(81)90059-4.
- [24] Sacha Davidson, Enrico Nardi, and Yosef Nir. Leptogenesis. *Phys. Rept.*, 466:105–177, 2008. doi: 10.1016/j.physrep.2008.06.002.
- [25] Guido Altarelli and Ferruccio Feruglio. Discrete Flavor Symmetries and Models of Neutrino Mixing. *Rev. Mod. Phys.*, 82:2701–2729, 2010. doi: 10.1103/RevModPhys.82.2701.
- [26] Asmaa Abada and Michele Lucente. Looking for the minimal inverse seesaw realisation. *Nucl. Phys. B*, 885:651–678, 2014. doi: 10.1016/j.nuclphysb.2014.06.003.
- [27] Sergey Alekhin et al. A facility to Search for Hidden Particles at the CERN SPS: the SHiP physics case. *Rept. Prog. Phys.*, 79(12):124201, 2016. doi: 10.1088/0034-4885/79/12/124201.
- [28] J. Hisano, T. Moroi, K. Tobe, and Masahiro Yamaguchi. Lepton flavor violation via right-handed neutrino Yukawa couplings in supersymmetric standard model. *Phys. Rev. D*, 53:2442–2459, 1996. doi: 10.1103/PhysRevD.53.2442.
- [29] Yoshitaka Kuno and Yasuhiro Okada. Muon decay and physics beyond the standard model. *Rev. Mod. Phys.*, 73:151–202, 2001. doi: 10.1103/RevModPhys.73.151.
- [30] J. Beacham et al. Physics Beyond Colliders at CERN: Beyond the Standard Model Working Group Report. *J. Phys. G*, 47(1):010501, 2020. doi: 10.1088/1361-6471/ab4cd2.
- [31] S. Navas et al. Review of particle physics. *Phys. Rev. D*, 110(3):030001, 2024. doi: 10.1103/PhysRevD.110.030001.
- [32] Gianfranco Bertone, Dan Hooper, and Joseph Silk. Particle dark matter: Evidence, candidates and constraints. *Phys. Rept.*, 405:279–390, 2005. doi: 10.1016/j.physrep.2004.08.031.
- [33] N. Aghanim et al. Planck 2018 results. VI. Cosmological parameters. *Astron. Astrophys.*, 641:A6, 2020. doi: 10.1051/0004-6361/201833910. [Erratum: *Astron. Astrophys.* 652, C4 (2021)].
- [34] D. N. Spergel et al. First year Wilkinson Microwave Anisotropy Probe (WMAP) observations: Determination of cosmological parameters. *Astrophys. J. Suppl.*, 148:175–194, 2003. doi: 10.1086/377226.
- [35] George F. Smoot et al. Structure in the COBE differential microwave radiometer first year maps. *Astrophys. J. Lett.*, 396:L1–L5, 1992. doi: 10.1086/186504.

- [36] Jonathan L. Feng. Dark Matter Candidates from Particle Physics and Methods of Detection. *Ann. Rev. Astron. Astrophys.*, 48:495–545, 2010. doi: 10.1146/annurev-astro-082708-101659.
- [37] Giorgio Arcadi, Maíra Dutra, Pradipta Ghosh, Manfred Lindner, Yann Mambrini, Mathias Pierre, Stefano Profumo, and Farinaldo S. Queiroz. The waning of the WIMP? A review of models, searches, and constraints. *Eur. Phys. J. C*, 78(3):203, 2018. doi: 10.1140/epjc/s10052-018-5662-y.
- [38] Gianfranco Bertone and Tim Tait, M. P. A new era in the search for dark matter. *Nature*, 562(7725):51–56, 2018. doi: 10.1038/s41586-018-0542-z.
- [39] Marco Cirelli, Alessandro Strumia, and Jure Zupan. Dark Matter. 6 2024.
- [40] Nassim Bozorgnia, Joseph Bramante, James M. Cline, David Curtin, David McKeen, David E. Morrissey, Adam Ritz, Simon Viel, Aaron C. Vincent, and Yue Zhang. Dark Matter Candidates and Searches. 9 2024. doi: 10.1139/cjp-2024-0128.
- [41] Csaba Balazs, Torsten Bringmann, Felix Kahlhoefer, and Martin White. A Primer on Dark Matter. 11 2024.
- [42] Brian Patt and Frank Wilczek. Higgs-field portal into hidden sectors. 5 2006.
- [43] Abdelhak Djouadi, Oleg Lebedev, Yann Mambrini, and Jeremie Quevillon. Implications of LHC searches for Higgs–portal dark matter. *Phys. Lett. B*, 709:65–69, 2012. doi: 10.1016/j.physletb.2012.01.062.
- [44] Fady Bishara, Joachim Brod, Patipan Uttayarat, and Jure Zupan. Nonstandard Yukawa Couplings and Higgs Portal Dark Matter. *JHEP*, 01:010, 2016. doi: 10.1007/JHEP01(2016)010.
- [45] Giorgio Arcadi, Abdelhak Djouadi, and Martti Raidal. Dark Matter through the Higgs portal. *Phys. Rept.*, 842:1–180, 2020. doi: 10.1016/j.physrep.2019.11.003.
- [46] Michael Dine, Willy Fischler, and Mark Srednicki. A Simple Solution to the Strong CP Problem with a Harmless Axion. *Phys. Lett. B*, 104:199–202, 1981. doi: 10.1016/0370-2693(81)90590-6.
- [47] R. D. Peccei and Helen R. Quinn. CP Conservation in the Presence of Instantons. *Phys. Rev. Lett.*, 38:1440–1443, 1977. doi: 10.1103/PhysRevLett.38.1440.
- [48] Steven Weinberg. A New Light Boson? *Phys. Rev. Lett.*, 40:223–226, 1978. doi: 10.1103/PhysRevLett.40.223.
- [49] Yasunori Nomura and Jesse Thaler. Dark Matter through the Axion Portal. *Phys. Rev. D*, 79:075008, 2009. doi: 10.1103/PhysRevD.79.075008.
- [50] Marat Freytsis, Zoltan Ligeti, and Jesse Thaler. Constraining the Axion Portal with $B \rightarrow Kl^+l^-$. *Phys. Rev. D*, 81:034001, 2010. doi: 10.1103/PhysRevD.81.034001.
- [51] Martin Bauer, Guillaume Rostagni, and Jonas Spinner. Axion-Higgs portal. *Phys. Rev. D*, 107(1):015007, 2023. doi: 10.1103/PhysRevD.107.015007.
- [52] Alexey S. Zhevlakov, Dmitry V. Kirpichnikov, and Valery E. Lyubovitskij. Implication of the dark axion portal for the EDM of fermions and dark matter probing with NA64e, NA64 μ , LDMX, M3, and BaBar. *Phys. Rev. D*, 106(3):035018, 2022. doi: 10.1103/PhysRevD.106.035018.

- [53] C. D. R. Carvajal, A. G. Dias, C. C. Nishi, and B. L. Sánchez-Vega. Axion Like Particles and the Inverse Seesaw Mechanism. *JHEP*, 05:069, 2015. doi: 10.1007/JHEP05(2015)069. [Erratum: JHEP 08, 103 (2015)].
- [54] B. Abi et al. Measurement of the Positive Muon Anomalous Magnetic Moment to 0.46 ppm. *Phys. Rev. Lett.*, 126(14):141801, 2021. doi: 10.1103/PhysRevLett.126.141801.
- [55] D. P. Aguillard et al. Measurement of the Positive Muon Anomalous Magnetic Moment to 0.20 ppm. *Phys. Rev. Lett.*, 131(16):161802, 2023. doi: 10.1103/PhysRevLett.131.161802.
- [56] G. W. Bennett et al. Final Report of the Muon E821 Anomalous Magnetic Moment Measurement at BNL. *Phys. Rev. D*, 73:072003, 2006. doi: 10.1103/PhysRevD.73.072003.
- [57] T. Aoyama et al. The anomalous magnetic moment of the muon in the Standard Model. *Phys. Rept.*, 887:1–166, 2020. doi: 10.1016/j.physrep.2020.07.006.
- [58] Sz. Borsanyi et al. Leading hadronic contribution to the muon magnetic moment from lattice QCD. *Nature*, 593(7857):51–55, 2021. doi: 10.1038/s41586-021-03418-1.
- [59] F. V. Ignatov et al. Measurement of the $e+e-\rightarrow\pi+\pi-$ cross section from threshold to 1.2 GeV with the CMD-3 detector. *Phys. Rev. D*, 109(11):112002, 2024. doi: 10.1103/PhysRevD.109.112002.
- [60] F. V. Ignatov et al. Measurement of the Pion Form Factor with CMD-3 Detector and its Implication to the Hadronic Contribution to Muon ($g-2$). *Phys. Rev. Lett.*, 132(23):231903, 2024. doi: 10.1103/PhysRevLett.132.231903.
- [61] Chuan-Hung Chen, Cheng-Wei Chiang, and Takaaki Nomura. Muon $g-2$ in a two-Higgs-doublet model with a type-II seesaw mechanism. *Phys. Rev. D*, 104(5):055011, 2021. doi: 10.1103/PhysRevD.104.055011.
- [62] R. Primulando, J. Julio, and P. Uttayarat. Minimal Zee model for lepton $g-2$ and W-mass shifts. *Phys. Rev. D*, 107(5):055034, 2023. doi: 10.1103/PhysRevD.107.055034.
- [63] Syuhei Iguro, Teppei Kitahara, Martin S. Lang, and Michihisa Takeuchi. Current status of the muon $g-2$ interpretations within two-Higgs-doublet models. *Phys. Rev. D*, 108(11):115012, 2023. doi: 10.1103/PhysRevD.108.115012.
- [64] João Paulo Pinheiro, C. A. de S. Pires, Farinaldo S. Queiroz, and Yoxara S. Villamizar. Confronting the inverse seesaw mechanism with the recent muon $g-2$ result. *Phys. Lett. B*, 823:136764, 2021. doi: 10.1016/j.physletb.2021.136764.
- [65] M. Ashry, K. Ezzat, and S. Khalil. Muon $g-2$ anomaly in a left-right model with an inverse seesaw mechanism. *Phys. Rev. D*, 107(5):055044, 2023. doi: 10.1103/PhysRevD.107.055044.
- [66] S. N. Gninenko and N. V. Krasnikov. The Muon anomalous magnetic moment and a new light gauge boson. *Phys. Lett. B*, 513:119, 2001. doi: 10.1016/S0370-2693(01)00693-1.
- [67] S. N. Gninenko and N. V. Krasnikov. Probing the muon $g_\mu - 2$ anomaly, $L_\mu - L_\tau$ gauge boson and Dark Matter in dark photon experiments. *Phys. Lett. B*, 783:24–28, 2018. doi: 10.1016/j.physletb.2018.06.043.
- [68] Manuel A. Buen-Abad, JiJi Fan, Matthew Reece, and Chen Sun. Challenges for an axion explanation of the muon $g - 2$ measurement. *JHEP*, 09:101, 2021. doi: 10.1007/JHEP09(2021)101.
- [69] Sougata Ganguly, Biswarup Mukhopadhyaya, and Sourov Roy. Can leptophilic-ALP be a solution to the muon ($g - 2$) anomaly? 4 2022.

- [70] Ryan Janish and Harikrishnan Ramani. Muon $g-2$ and EDM experiments as muonic dark matter detectors. *Phys. Rev. D*, 102:115018, 2020. doi: 10.1103/PhysRevD.102.115018.
- [71] Patrick deNiverville, Hye-Sung Lee, and Min-Seok Seo. Implications of the dark axion portal for the muon $g-2$, B factories, fixed target neutrino experiments, and beam dumps. *Phys. Rev. D*, 98(11):115011, 2018. doi: 10.1103/PhysRevD.98.115011.
- [72] Chakrit Pongkitivanichkul, Nakorn Thongyoi, and Patipan Uttayarat. Inverse seesaw mechanism and portal dark matter. *Phys. Rev. D*, 100(3):035034, 2019. doi: 10.1103/PhysRevD.100.035034.
- [73] Patrick J. Fitzpatrick, Yonit Hochberg, Eric Kuflik, Rotem Ovadia, and Yotam Soreq. Dark matter through the axion-gluon portal. *Phys. Rev. D*, 108(7):075003, 2023. doi: 10.1103/PhysRevD.108.075003.
- [74] Giovanni Armando, Paolo Panci, Joachim Weiss, and Robert Ziegler. Leptonic ALP portal to the dark sector. *Phys. Rev. D*, 109(5):055029, 2024. doi: 10.1103/PhysRevD.109.055029.
- [75] Dilip Kumar Ghosh, Anish Ghoshal, and Sk Jeessun. Axion-like particle (ALP) portal freeze-in dark matter confronting ALP search experiments. *JHEP*, 01:026, 2024. doi: 10.1007/JHEP01(2024)026.
- [76] Juan Cortabitarte Gutiérrez, Bradley J. Kavanagh, Núria Castelló-Mor, Francisco J. Casas, Jose M. Diego, Enrique Martínez-González, and Rocío Vilar Cortabitarte. Cosmology and direct detection of the Dark Axion Portal. 12 2021.
- [77] Francesco Paolo Di Meglio. Visible QCD Axion Portal to a Dark Sector. Master’s thesis, Pisa U., 2021.
- [78] Shivam Gola, Sanjoy Mandal, and Nita Sinha. ALP-portal majorana dark matter. *Int. J. Mod. Phys. A*, 37(22):2250131, 2022. doi: 10.1142/S0217751X22501317.
- [79] Patrick Deniverville, Hye-Sung Lee, and Young-Min Lee. New searches at reactor experiments based on the dark axion portal. *Phys. Rev. D*, 103(7):075006, 2021. doi: 10.1103/PhysRevD.103.075006.
- [80] D. V. Kirpichnikov, Valery E. Lyubovitskij, and Alexey S. Zhevlakov. Implication of hidden sub-GeV bosons for the $(g - 2)_\mu$, ^8Be - ^4He anomaly, proton charge radius, EDM of fermions, and dark axion portal. *Phys. Rev. D*, 102(9):095024, 2020. doi: 10.1103/PhysRevD.102.095024.
- [81] Patrick deNiverville and Hye-Sung Lee. Implications of the dark axion portal for SHiP and FASER and the advantages of monophoton signals. *Phys. Rev. D*, 100(5):055017, 2019. doi: 10.1103/PhysRevD.100.055017.
- [82] Kunio Kaneta, Hye-Sung Lee, and Seokhoon Yun. Dark photon relic dark matter production through the dark axion portal. *Phys. Rev. D*, 95(11):115032, 2017. doi: 10.1103/PhysRevD.95.115032.
- [83] Albert M Sirunyan et al. Measurements of Higgs boson production cross sections and couplings in the diphoton decay channel at $\sqrt{s} = 13$ TeV. *JHEP*, 07:027, 2021. doi: 10.1007/JHEP07(2021)027.
- [84] Georges Aad et al. A detailed map of Higgs boson interactions by the ATLAS experiment ten years after the discovery. *Nature*, 607(7917):52–59, 2022. doi: 10.1038/s41586-022-04893-w. [Erratum: *Nature* 612, E24 (2022)].
- [85] C. B. Adams et al. Axion Dark Matter. In *Snowmass 2021*, 3 2022.

- [86] Ivan Esteban, M. C. Gonzalez-Garcia, Michele Maltoni, Ivan Martinez-Soler, João Paulo Pinheiro, and Thomas Schwetz. NuFit-6.0: Updated global analysis of three-flavor neutrino oscillations. 10 2024.
- [87] Elizabeth Ellen Jenkins and Aneesh V. Manohar. Rephasing Invariants of Quark and Lepton Mixing Matrices. *Nucl. Phys. B*, 792:187–205, 2008. doi: 10.1016/j.nuclphysb.2007.09.031.
- [88] M. Aker et al. Direct neutrino-mass measurement based on 259 days of KATRIN data. 6 2024.
- [89] S. Abe et al. Search for the Majorana Nature of Neutrinos in the Inverted Mass Ordering Region with KamLAND-Zen. *Phys. Rev. Lett.*, 130(5):051801, 2023. doi: 10.1103/PhysRevLett.130.051801.
- [90] G. Belanger, F. Boudjema, A. Pukhov, and A. Semenov. micrOMEGAs: Recent developments. In *4th International Workshop on the Identification of Dark Matter*, pages 262–267, 10 2002. doi: 10.1142/9789812791313_0036.
- [91] G. Alguero, G. Belanger, F. Boudjema, S. Chakraborti, A. Goudelis, S. Kraml, A. Mjallal, and A. Pukhov. micrOMEGAs 6.0: N-component dark matter. *Comput. Phys. Commun.*, 299:109133, 2024. doi: 10.1016/j.cpc.2024.109133.
- [92] A. Semenov. LanHEP — A package for automatic generation of Feynman rules from the Lagrangian. Version 3.2. *Comput. Phys. Commun.*, 201:167–170, 2016. doi: 10.1016/j.cpc.2016.01.003.
- [93] Alexander Belyaev, Neil D. Christensen, and Alexander Pukhov. CalcHEP 3.4 for collider physics within and beyond the Standard Model. *Comput. Phys. Commun.*, 184:1729–1769, 2013. doi: 10.1016/j.cpc.2013.01.014.
- [94] M. Ajello et al. Search for Spectral Irregularities due to Photon–Axionlike-Particle Oscillations with the Fermi Large Area Telescope. *Phys. Rev. Lett.*, 116(16):161101, 2016. doi: 10.1103/PhysRevLett.116.161101.
- [95] H. Abdallah et al. Search for γ -Ray Line Signals from Dark Matter Annihilations in the Inner Galactic Halo from 10 Years of Observations with H.E.S.S. *Phys. Rev. Lett.*, 120(20):201101, 2018. doi: 10.1103/PhysRevLett.120.201101.
- [96] H. Abe et al. Search for Gamma-Ray Spectral Lines from Dark Matter Annihilation up to 100 TeV toward the Galactic Center with MAGIC. *Phys. Rev. Lett.*, 130(6):061002, 2023. doi: 10.1103/PhysRevLett.130.061002.
- [97] D. P. et al Aguilard. Measurement of the positive muon anomalous magnetic moment to 0.20 ppm. *Physical Review Letters*, 131(16), October 2023. ISSN 1079-7114. doi: 10.1103/physrevlett.131.161802. URL <http://dx.doi.org/10.1103/PhysRevLett.131.161802>.
- [98] Joshua W. Foster, Yujin Park, Benjamin R. Safdi, Yotam Soreq, and Weishuang Linda Xu. Search for dark matter lines at the Galactic Center with 14 years of Fermi data. *Phys. Rev. D*, 107(10):103047, 2023. doi: 10.1103/PhysRevD.107.103047.
- [99] S. Abe et al. Dark matter line searches with the Cherenkov Telescope Array. *JCAP*, 07:047, 2024. doi: 10.1088/1475-7516/2024/07/047.
- [100] Maximilian H. Abitbol et al. The Simons Observatory: Astro2020 Decadal Project Whitepaper. *Bull. Am. Astron. Soc.*, 51:147, 2019.

- [101] B. Alpert et al. HOLMES - The Electron Capture Decay of ^{163}Ho to Measure the Electron Neutrino Mass with sub-eV sensitivity. *Eur. Phys. J. C*, 75(3):112, 2015. doi: 10.1140/epjc/s10052-015-3329-5.
- [102] M. Aker et al. Improved Upper Limit on the Neutrino Mass from a Direct Kinematic Method by KATRIN. *Phys. Rev. Lett.*, 123(22):221802, 2019. doi: 10.1103/PhysRevLett.123.221802.
- [103] N. Abgrall et al. The Large Enriched Germanium Experiment for Neutrinoless Double Beta Decay (LEGEND). *AIP Conf. Proc.*, 1894(1):020027, 2017. doi: 10.1063/1.5007652.
- [104] G. Bernardi et al. The Future Circular Collider: a Summary for the US 2021 Snowmass Process. 3 2022.